Published in final edited form as:
Obesity (Silver Spring). 2010 April ; 18(4): 841–847. doi:10.1038/oby.2009.352.

Comparison of Fat–Water MRI and Single-voxel MRS in the Assessment of Hepatic and Pancreatic Fat Fractions in Humans

Houchun H. Hu[1], **Hee-Won Kim**[2], **Krishna S. Nayak**[1], and **Michael I. Goran**[3,4,5]

[1] Magnetic Resonance Engineering Laboratory, Ming Hsieh Department of Electrical Engineering, Viterbi School of Engineering, University of Southern California, Los Angeles, California, USA

[2] Department of Radiology, Keck School of Medicine, University of Southern California, Los Angeles, California, USA

[3] Department of Preventive Medicine, Keck School of Medicine, University of Southern California, Los Angeles, California, USA

[4] Department of Physiology and Biophysics, Keck School of Medicine, University of Southern California, Los Angeles, California, USA

[5] Department of Pediatrics, Keck School of Medicine, University of Southern California, Los Angeles, California, USA

Abstract

The ability to accurately and noninvasively quantify fatty infiltration in organs such as the liver and the pancreas remains a critical component in understanding the link between obesity and its comorbidities such as type 2 diabetes and fatty liver disease. Single-voxel (^{1}H) proton magnetic resonance spectroscopy (MRS) has long been regarded as the gold-standard noninvasive technique for such measurements. Recent advances in three-dimensional fat–water magnetic resonance imaging (MRI) methods have led to the development of rapid, robust, and quantitative approaches that can accurately characterize the proportion of fat and water content in underlying tissues across the full imaging volume, and hence entire organs of interest. One such technique is called IDEAL (Iterative Decomposition with Echo Asymmetry and Least squares estimation). This article prospectively compares three-dimensional (3D) IDEAL-MRI and single-voxel MRS in the assessment of hepatic (HFF) and pancreatic fat fraction (PFF) in 16 healthy subjects. MRS acquisitions took 3–4 min to complete whereas IDEAL acquisitions were completed in 20-s breath-holds. In the liver, there was a strong correlation (slope = 0.90, $r^2 = 0.95$, $P < 0.001$) between IDEAL and MRS-based fat fractions. In the pancreas, a poorer agreement between IDEAL and MRS was observed (slope = 0.32, $r^2 = 0.51$, $P < 0.02$). The discrepancy of PFF is likely explained by MRS signal contamination from surrounding visceral fat, presumably during respiratory motion. We conclude that IDEAL is equally accurate in characterizing hepatic fat content as MRS, and is potentially better suited for fat quantification in smaller organs such as the pancreas.

INTRODUCTION

Obesity continues to be a growing health concern in the United States, affecting multiple health outcomes in children, adolescents, and adults (1). Increased health risks of obesity include multiple cardiovascular and metabolic disorders. Many of these risks are hypothesized to be

Correspondence: Houchun H. Hu (houchunh@usc.edu).

Disclosure

The authors declared no conflict of interest.

mainly attributed to the build-up of visceral and organ (ectopic) fat (2–5). Therefore, the accurate, quantitative, and noninvasive assessment of adipose tissue depots and fatty infiltration in critical organs such as the liver and the pancreas remains a critical component in both obesity research and clinical management.

Magnetic resonance imaging (MRI) is well-suited for fat quantification (6–8) because it is noninvasive and provides sensitive mechanisms for differentiating fat from lean tissues based on T_1 relaxation and chemical-shift properties. Furthermore, it does not utilize ionizing radiation, has unlimited repeatability, and is safe for use in children. Magnetic resonance spectroscopy (MRS) is generally considered the clinical gold-standard noninvasive technique for *in vivo* fat and metabolite quantification. It is routinely used for measuring liver fat (9–11), myocellular lipids (12), tissue composition (13), and brain metabolites. In 1984, Dixon described a two-dimensional imaging approach that exploited the chemical-shift difference between protons in water and fat to separate the two moieties (14). Over the past 25 years, Dixon's method has evolved significantly (15–17), and recent advances in reconstruction algorithms have led to the development of a fat–water three-dimensional (3D) imaging technique called IDEAL (Iterative Decomposition with Echo Asymmetry and Least squares estimation) (18,19). IDEAL is particularly robust to resonance offsets (off-resonance due to magnetic field nonuniformity, a common system imperfection), and produces separated fat and water images that are optimal in terms of signal-to-noise ratio (20).

Both MRS and IDEAL utilize chemical-shift principles, where the resonant frequencies of protons of water and of the primary methylene groups $(–CH_2)_n–$ of triglyceride fatty acid chains are separated by ~3.4 p.p.m. This results in a net difference in resonant frequency that is dependent on the magnetic field. Whereas water is characterized by a single spectral peak, fat has several additional minor peaks, including methyl, olenific, and carboxyl groups, which all have slightly different chemical shifts with respect to water (21). One major difference between MRS and IDEAL-MRI is that MRS is limited to a single voxel of interest (1–8 cm^3) per data acquisition. Although single-voxel MRS yields direct information about the presence and quantity of chemical species with high spectral resolution, it does not provide any spatial image information. In contrast, IDEAL is a 3D imaging technique. It provides very accurate measures of the proton ratio between fat and water in underlying tissues. In particular, multi-fat-peak T^*_2-IDEAL (22) yields an improved fat-to-water ratio by systematically accounting for transverse relaxation and intravoxel dephasing effects in the acquired MRI signal, scanner imperfections such as magnetic field nonuniformity, and the multiple spectral peaks of fat. The resulting ratio can then be used to quantify the relative amounts of fat in specific regions of interest, such as fat depots and organs, on a voxel-wise basis across the entire 3D imaging volume.

The purpose of this work is to prospectively evaluate and compare multi-fat-peak T^*_2-IDEAL against single-voxel proton MRS in the assessment of hepatic (HFFs) and pancreatic fat fractions (PFFs). We hypothesize that IDEAL and MRS fat fractions will correlate strongly in both the liver and the pancreas. Furthermore, we will demonstrate that IDEAL has several advantages over MRS: it is able to provide high-resolution contiguous images of the abdomen in breath-hold durations; it is not limited by a single voxel of interest; its intrinsic 3D imaging capability allows whole organs and spatial variations in ectopic fat across any region of the imaged anatomy to be evaluated.

METHODS AND PROCEDURES

All experiments were performed on a 3-Tesla whole-body human MRI scanner (Signa HDx; GE Healthcare, Waukesha, WI). Phantom experimental data were acquired with a single-channel transmit/receive head coil. Human data were acquired with an eight-channel receive-

only abdominal torso array. An investigational version of the IDEAL software was installed on the scanner. The study was approved by the local institutional review board, followed all informed consent guidelines, and was Health Insurance Portability and Accountability Act-compliant.

3D IDEAL fat–water MRI

The IDEAL imaging and reconstruction method is the latest generalization of the Dixon technique (14) for separating water W and fat F components using chemical-shift MRI. We utilized T^*_2-IDEAL with fat spectrum modeling (22), based on the signal model in Eq. (1),

$$s(t)=\left(W+F\sum a_i \bullet e^{j2\pi t(\Delta f_i)}\right)e^{j2\pi t\psi-\left(t/T_2^*\right)} \quad (1)$$

where $s(t)$ represents the signal acquired at time t in a given voxel, Δf_i and a_i are the chemical-shift spectral frequency and relative amplitude of the ith spectral peak of F relative to W, ψ describes the magnetic field inhomogeneity, j is the imaginary number (square root of −1), and T^*_2 characterizes transverse relaxation and intravoxel dephasing of the signal. The unknown parameters (W, F, ψ, T^*_2) are solved iteratively with six measurements of $s(t)$ (22). The resulting IDEAL fat fraction (FF) is computed from the separated water and fat signals (Eq. (2)) on a voxel-by-voxel basis. The accuracy of the fat fraction metric from multi-fat-peak T^*_2-IDEAL and other similar multi-echo fat quantification methods has been validated in several hepatic fat quantification studies (23–26).

$$\text{Fat fraction}(\text{FF})_{\text{IDEAL}} = \frac{F}{(W+F)} \times 100\%$$

Single-voxel proton MRS

In this work, the point-resolved spectroscopy method was utilized (27). MRS data acquisition typically requires placement of a single large voxel (≈1–8 cm^3) in an anatomical region-of-interest. Postprocessing and quantification generally involves noise filtering, apodization, baseline, and phase correction, signal fitting of the peaks within the acquired spectra, and integration to find the area under each spectral peak of interest (e.g., water at 4.7 p.p.m., methylene fat at 1.3 p.p.m.). We used the Java-based MRUI software package (http://sermn02.uab.cat/mrui/) (28,29) for spectral quantification. Subsequently, the MRS fat fraction is defined by Eq. (3).

$$\text{Fat fraction (FF)}_{\text{MRS}} = \frac{\text{area under fat peaks}}{(\text{area under fat and water peaks})} \times 100\%$$

Phantom validation

We first evaluated the accuracy of the FF_{IDEAL} in a set of known standards. Homogeneous emulsions consisting of vegetable (corn) oil and distilled and un-doped water were prepared (Figure 1) in 60-ml bottles across 0–100% fat volume fractions, similar to the setup previously described by Bernard *et al.* (30). Agar gel (2% by weight) and dioctyl sulfosuccinate sodium salt (Alfa Aesar, Ward Hill, MA) were used to stabilize the emulsions. The emulsions were prepared slowly over a heat-stir plate and subsequently cooled to allow the suspension to stay

intact. A 3D multi-fat-peak T^*_2-IDEAL spoiled-gradient-echo pulse sequence was used with the following parameters, repetition time = 10 ms, echo times = (2.0, 2.4, 2.8, 3.2, 3.6, 4.0) ms, flip angle = 5°, receiver bandwidth = ±125 kHz, 2 mm in-plane spatial resolution (160 × 160 sampling matrix), eight 5-mm slices, and a single signal average. The bottles were placed in a bowl filled with additional water. Single voxel MRS was additionally performed on four emulsions (10, 30, 60, and 80% fat) with scan parameters described in the following section.

In vivo experiments

A cohort of 16 healthy and asymptomatic subjects was enrolled for the prospective *in vivo* study (7 men, 9 female, age range: 24–54 years). Each subject underwent an MRI examination that involved first a set of localizer images. This was followed by a single axial 3D IDEAL spoiled-gradient-echo acquisition encompassing the right lobe of the liver. The imaging parameters were similar to those of the phantom study, except in-plane resolution varied between 2 and 2.75 mm, depending on body habitus, and 12 slices were acquired. A total of six echoes were acquired, using an echo spacing of 0.8 ms and with the first echo between 1.0 to 1.5 ms. The IDEAL scan required a 20-s breath-hold. In eight subjects, the pancreas was also included in the imaging volume and could be easily identified. Following IDEAL, the examination also included MRS acquisitions of the liver ($n = 16$) and the pancreas ($n = 8$). MRS parameters included: repetition time = 4 s, echo time = 23 ms, 2,048 data points, 2,500 Hz bandwidth, no water suppression, and eight signal averages. For the liver, a 20 × 20 × 20-mm^3 voxel was placed in the right lobe and care was taken to avoid any vascular and biliary structures. For the pancreas, the largest voxel that could be placed within the organ was used. During prescription based on the localizer images, the operator carefully placed the voxel at a location that excluded any visceral fat surrounding the pancreas. Pancreas voxel size range was from 10 × 10 × 8 mm^3 to 10 × 20 × 12 mm^3. Each MRS scan took ~3–4 min to complete, during which the subject breathed freely, and no respiratory gating was used. For demonstration purposes, we additionally performed IDEAL imaging across the whole abdomen in two participants. This involved a total of five 20-s breath-holds with an imaging volume that extended from the top of the liver to the iliac crest.

Data and statistical analysis

IDEAL (FF_{IDEAL}) and MRS (FF_{MRS}) fat fractions were compared against true fat volume fractions in the phantom experiment using linear correlation. For *in vivo* studies, IDEAL results were correlated against MRS fat fractions. Specifically for each participant, the mean FF_{IDEAL} within each organ closely matching the locations of the MRS voxels were compared against FF_{MRS}. Regions were manually segmented based on the IDEAL fat fraction maps, and excluded vascular and nontissue structures. Linear correlation, Pearson's product–moment correlation coefficient (r), and Bland–Altman analyses were used to compare IDEAL and MRS in estimating HFFs and PFFs. For linear correlation, we tested whether the resultant slope was significantly different from zero using the t-test. For Bland–Altman plots, we tested whether the differences between IDEAL and MRS was statistically significantly from zero using the paired t-test. $P < 0.05$ was used to conclude statistical significance and 95% confidence intervals are provided for the *in vivo* experiments.

Results

Phantom validation

Figure 1 summarizes results from the phantom experiment. Separated water, fat, and fat fraction images from IDEAL are illustrated, demonstrating different amounts of each component in the various emulsions. A plot comparing the true fat volume fraction against FF_{IDEAL} yielded excellent correlation (slope = 1.01, $r^2 = 0.99$, $P < 0.001$), with a very slight bias at the zero-intercept of 0.09% that is not significantly different from zero. This residual is likely due to

intrinsic noise in the separated fat and water image, phase errors due to eddy currents from the magnet hardware, and that the fat fraction operation in Eq. (2) utilizes magnitude values of *F* and *W*. This suggests that the IDEAL technique is robust in fat–water separation and accurate in quantifying fat content across the entire fat fraction range. The correlation between true fat volume fraction and FF_{MRS} was similarly strong.

Figure 2 illustrates HFF results from two subjects, one with a lean liver (top row), and one with a fatty liver (bottom row). Excellent fat and water separation is achieved in both subjects. Associated MRS plots are also shown, corresponding to the white voxel highlighted in the each fat fraction map. HFF_{IDEAL} and HFF_{MRS} are in close agreement, and differences between the fat fraction maps within the liver and the spectra of the two subjects are apparent. Figure 3a,b summarizes HFF results from all 16 studies. A strong agreement and correlation between HFF_{IDEAL} and HFF_{MRS} was obtained (slope = 0.90, intercept = 1.07%, $r^2 = 0.95$, $P < 0.001$), as shown in Figure 3a. The 95% confidence interval for the slope was 0.82–0.98. The 95% confidence interval for the intercept was −1.10–3.25. Figure 3b illustrates the associated Bland–Altman plot, where the dashed lines represent the 95% confidence interval. The average difference between HFF_{MRS} and HFF_{IDEAL} was 0.38% (range: −4.1 to 2.9%). This was not significantly different from zero (95% confidence interval: −3.5 to 4.3, $P < 0.4$).

Figure 3c,d summarizes PFF results. The strength of agreement between PFF_{MRS} and PFF_{IDEAL} was weaker, though the correlation was still statistically significant (slope = 0.32, intercept = 2.74%, $r^2 = 0.51$, $P < 0.02$). The 95% confidence interval for the slope spans a broad range from 0.10 to 0.53. The 95% confidence interval for the intercept was 0.97–4.50. In cases where MRS and IDEAL measurements differed, MRS showed a tendency to produce higher PFF values. Figure 3d illustrates the corresponding Bland–Altman plot. The average difference between PFF_{IDEAL} and PFF_{MRS} was 2.7% (range: −1.3 to 8%), and was very close to being statistically different from zero (95% confidence interval: −4 to 9.3, $0.05 < P < 0.1$).

Figure 4 illustrates a coronal reformation of the whole abdomen from one of the subjects. Axial IDEAL acquisitions were performed five times, each requiring a 20-s breath-hold. The imaging volume provided contiguous coverage from the top of the liver to the iliac crest. The abdominal fat fraction map clearly highlights subcutaneous, visceral, and mesenteric adipose tissue depots. Two exemplary native axial slices are shown, one at the level of the liver and the pancreas, and one at the level of the kidneys. Note the abundance of visceral adipose tissues surrounding the elongated pancreas. A line profile is drawn through the liver from the bottom of the organ (inferior) to the top (superior) in the coronal reformat. The line profile shows nonuniform fat fractions across the organ, providing an example of how IDEAL can potentially detect heterogeneous organ fat infiltrations with millimeter spatial resolution.

DISCUSSION

We have demonstrated a strong potential for rapid breath-hold 3D multi-fat-peak T^*_2-IDEAL as a fat quantification tool, and propose the method as a valuable tool for obesity research. In phantoms, we have shown that the IDEAL fat fraction, a ratio that intrinsically represents the content of fat and water protons, also correlates strongly with the underlying fat volume fraction in a set of emulsion standards (Figure 1). The robust relationship between the fat fraction metric and fat volume fraction has been verified by other investigators (31,32). In the *in vivo* experiments, excellent correlation was achieved between FF_{IDEAL} and FF_{MRS} in the liver (Figure 3). In the measurement of PFF, only a moderate correlation was obtained between FF_{IDEAL} and FF_{MRS}. In six out of the eight pancreas data points, MRS estimates were greater than the IDEAL fat fraction (Figure 3c).

We attribute the poor correlation in the pancreas to two reasons. First, placement of an MRS voxel requires operator expertise, due to the small organ's elongated shape. Voxel prescription is performed on localizer images that are acquired after subject placement within the scanner bore. In our study, pancreas MRS was acquired several minutes after the localizers. During this period, slight motion of the subject could have caused a spatial mismatch between the prescribed voxel and the anatomy. Second, abdominal organs shift during respiration (33,34). In our experience, we have observed the pancreas to shift ~15 mm along the superior–inferior axis between inspiration and expiration due to diaphragm motion. Respiratory motion can therefore lead to erroneous fat signal contamination of the MRS spectra from the abundance of visceral fat surrounding the pancreas (Figure 4). In contrast, a liver MRS voxel can be placed such that the voxel remains confidently within the organ throughout the respiratory cycle.

In a report by Tushuizen *et al.*, the coefficient of variation from test–retest of pancreatic MRS was 15.2% in comparison to liver MRS (4.7%) (ref. 35). The authors reported individual pancreas spectra on occasion exhibited dramatic increases in the fat signal, and attributed such observations to sudden deep breathing of the subject. We observed similar occurrences in this study. Although respiration can be monitored with a bellows transducer to synchronize MRS acquisition with the subject's breathing motion (36), gating can further increase scan time, which may cause subject discomfort. It may also not be possible to use in subjects with a large body habitus.

Although the IDEAL algorithm employed in this work accounted for transverse relaxation and intravoxel dephasing (T_2, T^*_2) by acquiring six echoes, we did not perform similar T_2 corrections for MRS. Our MRS protocol used a single echo time of 23 ms. For T_2 correction, additional spectra at several other echo times would have been required at the expense of increasing scan time. Alternatively, MRS scan time can be reduced by using a single signal average. We utilized eight averages in this work to ensure adequate signal-to-noise ratio and minimal baseline variations in the acquired spectra. Nonetheless, with additional correction for T_2, the correlation between IDEAL and MRS in the liver (Figure 3a) could have been even closer to identity. Recent work has also emphasized T_2 correction in computing accurate FF_{MRS} (37). In both IDEAL and MRS protocols used in this work, minimization of the longitudinal relaxation (T_1-bias) was considered, and was achieved by using a 5° flip angle (31,38) and a repetition time of 4 s (8,37), respectively.

IDEAL-MRI has several advantages over MRS. IDEAL can be easily performed within a breath-hold and does not require respiratory gating. It does not require a high-level of operator expertise in voxel prescription. The quantitative end point is a voxel-wise fat fraction map of the entire abdomen (Figure 4) that can potentially show heterogeneous distributions and spatial patterns of ectopic fat, along with 3D contiguous anatomical images of the fat and water components (Figure 2). In this work, IDEAL image reconstruction and fat fraction computation was performed online on the scanner host computer immediately after data acquisition, and took ~2–3 min. Subsequently, manual segmentation of the liver and the pancreas was performed on the fat fraction maps, and care was taken to avoid hepatic vessels and nontissue structures. The benefits and attractiveness of IDEAL in fat quantification have been recognized, and validation studies in several large patient cohorts have been recently reported (23–26).

The IDEAL approach described in this work has some limitations. First, in order to capture the entire abdomen, it requires multiple breath-holds, which may not be realizable in certain patient groups. Second, the reconstruction algorithm requires an accurate model of the fat spectra. In Eq. (1), IDEAL requires a prior knowledge of Δf_i and a_i values, and utilizes these to reconstruct images of water, fat, and the fat fraction map. In its current implementation, Δf_i and a_i values are determined based on subcutaneous adipose tissue (13,22). Potential inaccuracies in the fat fraction map may result if the lipid spectral profiles of triglycerides in

organs are significantly different from that of subcutaneous adipose tissue. Nonetheless, accurate fat spectral modeling has recently been shown to be a very critical component of accurate fat fraction estimation (26). Third, the signal model in Eq. (1) assumes a common T^*_2 value for both water and fat components. To improve accuracy further, individual water and fat T^*_2 relaxation terms should be adopted (39), which will potentially require the acquisition of >6 echoes to solve the system of equations in Eq. (1) robustly.

In conclusion, 3D IDEAL-MRI is a rapid breath-hold technique that provides robust separation of fat–water signals and accurate estimation of fat fractions. Unlike single-voxel MRS, IDEAL provides greater spatial resolution and anatomical detail, is much less susceptible to respiratory motion effects, and facilitates assessment of fat content in smaller organs, such as the pancreas. IDEAL has the potential to replace gold-standard MRS for noninvasive fat quantification in both clinical and obesity research protocols.

Acknowledgments

H.H.H. and K.S.N. acknowledge NCI Centers for Transdisciplinary Research on Energetics and Cancer (TREC) (U54 CA 116848) and NIDDK (R21 DK 081173) for funding support. This work was also supported by the Dr Atkins Foundation. We also thank Dr. Gavin Hamilton from the University of California, San Diego, for assistance with the Java-based MRUI software. We also acknowledge Dr Huanzhou Yu and Ann Shimakawa from GE Healthcare for providing the IDEAL software and technical research support.

References

1. Ogden CL, Carroll MD, Curtin LR, et al. Prevalence of overweight and obesity in the United States, 1999–2004. JAMA 2006;295:1549–1555. [PubMed: 16595758]
2. Després JP. Cardiovascular disease under the influence of excess visceral fat. Crit Pathw Cardiol 2007;6:51–59. [PubMed: 17667865]
3. Bergman RN, Kim SP, Hsu IR, et al. Abdominal obesity: role in the pathophysiology of metabolic disease and cardiovascular risk. Am J Med 2007;120:S3–S8. discussion S29. [PubMed: 17296343]
4. Després JP, Lemieux I, Bergeron J, et al. Abdominal obesity and the metabolic syndrome: contribution to global cardiometabolic risk. Arterioscler Thromb Vasc Biol 2008;28:1039–1049. [PubMed: 18356555]
5. Mathieu P, Pibarot P, Larose E, et al. Visceral obesity and the heart. Int J Biochem Cell Biol 2008;40:821–836. [PubMed: 18201922]
6. Machann J, Thamer C, Schnoedt B, et al. Standardized assessment of whole body adipose tissue topography by MRI. J Magn Reson Imaging 2005;21:455–462. [PubMed: 15778954]
7. Siegel MJ, Hildebolt CF, Bae KT, Hong C, White NH. Total and intraabdominal fat distribution in preadolescents and adolescents: measurement with MR imaging. Radiology 2007;242:846–856. [PubMed: 17244720]
8. Cassidy FH, Yokoo T, Aganovic L, et al. Fatty liver disease: MR imaging techniques for the detection and quantification of liver steatosis. Radiographics 2009;29:231–260. [PubMed: 19168847]
9. Longo R, Pollesello P, Ricci C, et al. Proton MR spectroscopy in quantitative *in vivo* determination of fat content in human liver steatosis. J Magn Reson Imaging 1995;5:281–285. [PubMed: 7633104]
10. Kim H, Taksali SE, Dufour S, et al. Comparative MR study of hepatic fat quantification using single-voxel proton spectroscopy, two-point Dixon and three-point IDEAL. Magn Reson Med 2008;59:521–527. [PubMed: 18306404]
11. Thomsen C, Becker U, Winkler K, et al. Quantification of liver fat using magnetic resonance spectroscopy. Magn Reson Imaging 1994;12:487–495. [PubMed: 8007779]
12. Machann J, Bachmann OP, Brechtel K, et al. Lipid content in the musculature of the lower leg assessed by fat selective MRI: intra- and interindividual differences and correlation with anthropometric and metabolic data. J Magn Reson Imaging 2003;17:350–357. [PubMed: 12594726]
13. Ren J, Dimitrov I, Sherry AD, Malloy CR. Composition of adipose tissue and marrow fat in humans by ^{1}H NMR at 7 Tesla. J Lipid Res 2008;49:2055–2062. [PubMed: 18509197]

14. Dixon WT. Simple proton spectroscopic imaging. Radiology 1984;153:189–194. [PubMed: 6089263]
15. Glover GH, Schneider E. Three-point Dixon technique for true water/fat decomposition with B0 inhomogeneity correction. Magn Reson Med 1991;18:371–383. [PubMed: 2046518]
16. Hardy PA, Hinks RS, Tkach JA. Separation of fat and water in fast spin-echo MR imaging with the three-point Dixon technique. J Magn Reson Imaging 1995;5:181–185. [PubMed: 7766980]
17. Xiang QS. Two-point water-fat imaging with partially-opposed-phase (POP) acquisition: an asymmetric Dixon method. Magn Reson Med 2006;56:572–584. [PubMed: 16894578]
18. Reeder SB, Pineda AR, Wen Z, et al. Iterative decomposition of water and fat with echo asymmetry and least-squares estimation (IDEAL): application with fast spin-echo imaging. Magn Reson Med 2005;54:636–644. [PubMed: 16092103]
19. Reeder SB, McKenzie CA, Pineda AR, et al. Water-fat separation with IDEAL gradient-echo imaging. J Magn Reson Imaging 2007;25:644–652. [PubMed: 17326087]
20. Pineda AR, Reeder SB, Wen Z, Pelc NJ. Cramér-Rao bounds for three-point decomposition of water and fat. Magn Reson Med 2005;54:625–635. [PubMed: 16092102]
21. Brix G, Heiland S, Bellemann ME, Koch T, Lorenz WJ. MR imaging of fat-containing tissues: valuation of two quantitative imaging techniques in comparison with localized proton spectroscopy. Magn Reson Imaging 1993;11:977–991. [PubMed: 8231682]
22. Yu H, Shimakawa A, McKenzie CA, et al. Multiecho water-fat separation and simultaneous R2* estimation with multifrequency fat spectrum modeling. Magn Reson Med 2008;60:1122–1134. [PubMed: 18956464]
23. Yokoo T, Bydder M, Hamilton G, et al. Nonalcoholic fatty liver disease: diagnostic and fat-grading accuracy of low-flip-angle multiecho gradient-recalled-echo MR imaging at 1.5 T. Radiology 2009;251:67–76. [PubMed: 19221054]
24. Shiehmorteza M, Yokoo T, Hamilton G, et al. Hepatic fat quantification in children using multi-echo gradient-echo imaging and fat spectral modeling at 1.5 T. 17th Meeting of the International Society of Magnetic Resonance in Medicine 2009;17:204.
25. Meisamy S, Hines CDG, Hamilton G, et al. Validation of chemical shift based fat-fraction imaging with MR spectroscopy. 17th Meeting of the International Society of Magnetic Resonance in Medicine 2009;17:207.
26. Reeder SB, Robson PM, Yu H, et al. Quantification of hepatic steatosis with MRI: the effects of accurate fat spectral modeling. J Magn Reson Imaging 2009;29:1332–1339. [PubMed: 19472390]
27. Bottomley PA. Spatial localization in NMR spectroscopy in vivo. Ann N Y Acad Sci 1987;508:333–348. [PubMed: 3326459]
28. Naressi A, Couturier C, Devos JM, et al. Java-based graphical user interface for the MRUI quantitation package. MAGMA 2001;12:141–152. [PubMed: 11390270]
29. Naressi A, Couturier C, Castang I, de Beer R, Graveron-Demilly D. Java-based graphical user interface for MRUI, a software package for quantitation of *in vivo*/medical magnetic resonance spectroscopy signals. Comput Biol Med 2001;31:269–286. [PubMed: 11334636]
30. Bernard CP, Liney GP, Manton DJ, Turnbull LW, Langton CM. Comparison of fat quantification methods: a phantom study at 3.0T. J Magn Reson Imaging 2008;27:192–197. [PubMed: 18064714]
31. Bydder M, Yokoo T, Hamilton G, et al. Relaxation effects in the quantification of fat using gradient echo imaging. Magn Reson Imaging 2008;26:347–359. [PubMed: 18093781]
32. Reeder SB, Hines CDG, Yu H, McKenzie CA, Brittain J. On the definition of fat-fraction for in vivo fat quantification with magnetic resonance imaging. 17th Meeting of the International Society of Magnetic Resonance in Medicine 2009;17:211.
33. Nehrke K, Börnert P, Manke D, Böck JC. Free-breathing cardiac MR imaging: study of implications of respiratory motion—initial results. Radiology 2001;220:810–815. [PubMed: 11526286]
34. Manke D, Rösch P, Nehrke K, Börnert P, Dössel O. Model evaluation and calibration for prospective respiratory motion correction in coronary MR angiography based on 3-D image registration. IEEE Trans Med Imaging 2002;21:1132–1141. [PubMed: 12564881]
35. Tushuizen ME, Bunck MC, Pouwels PJ, et al. Pancreatic fat content and β-cell function in men with and without type 2 diabetes. Diabetes Care 2007;30:2916–2921. [PubMed: 17666465]

36. Lingvay I, Price AL, Legendre J, Sen S, Szczepaniak LS. Localized MRS of Human Pancreas. 17th Meeting of the International Society of Magnetic Resonance in Medicine 2009;17:472.

37. Sharma P, Martin DR, Pineda N, et al. Quantitative analysis of T2-correction in single-voxel magnetic resonance spectroscopy of hepatic lipid fraction. J Magn Reson Imaging 2009;29:629–635. [PubMed: 19243059]

38. Liu CY, McKenzie CA, Yu H, Brittain JH, Reeder SB. Fat quantification with IDEAL gradient echo imaging: correction of bias from T(1) and noise. Magn Reson Med 2007;58:354–364. [PubMed: 17654578]

39. O'Regan DP, Callaghan MF, Wylezinska-Arridge M, et al. Liver fat content and T2*: simultaneous measurement by using breath-hold multiecho MR imaging at 3.0 T—feasibility. Radiology 2008;247:550–557. [PubMed: 18349314]

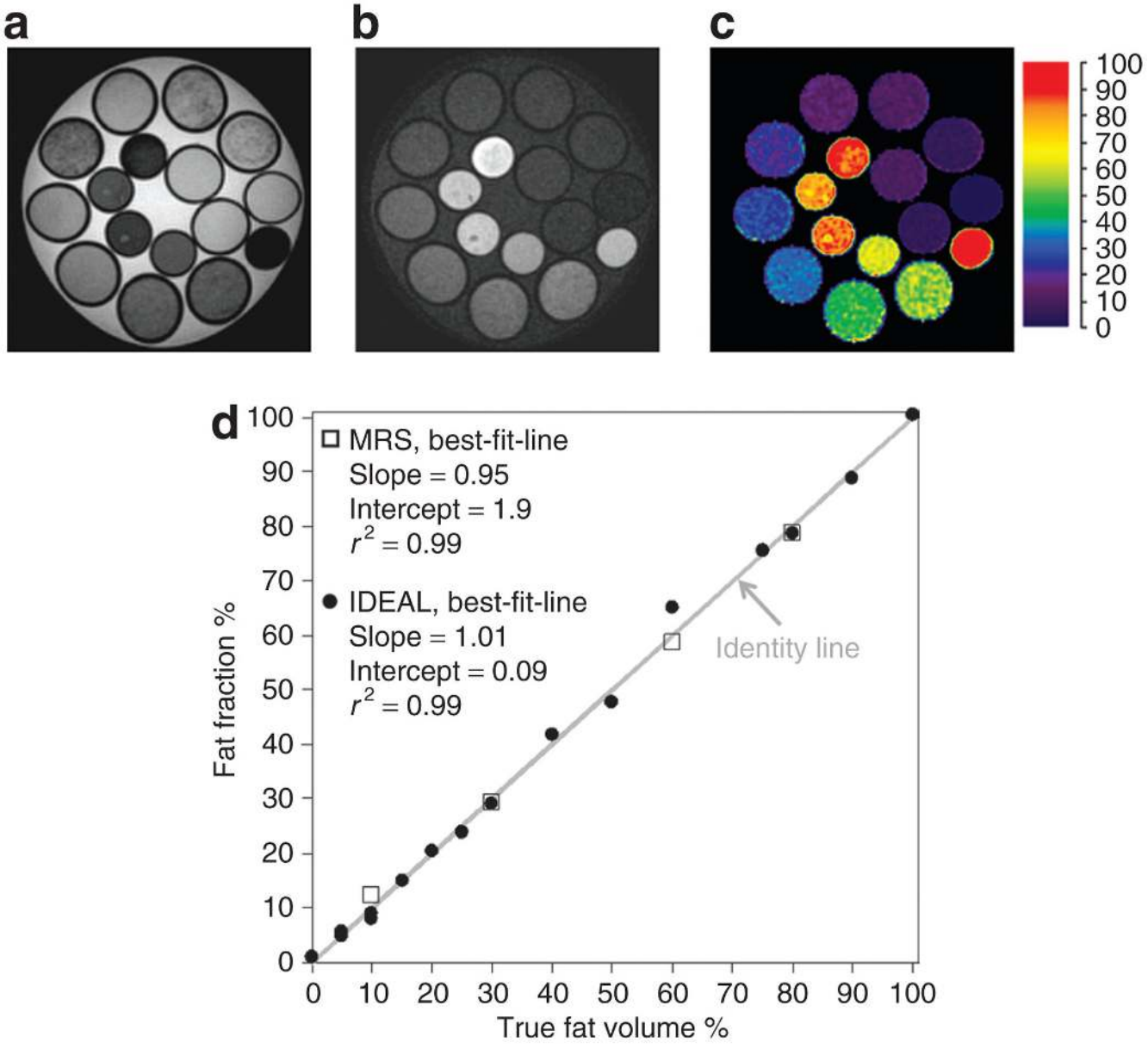

Figure 1.

Results from oil–water emulsion experiment. Reconstructed (**a**) water, (**b**) fat, and (**c**) fat fraction images demonstrate excellent fat and water separation and show clear differences in the amounts of fat and water in each vial. (**d**) Correlation of true fat volume fraction against the mean fat fraction computed from IDEAL (circle) and MRS (open square) is strong across the full fat fraction range. The best-fit-lines are not shown because they nearly overlap the identity line (gray). Note that water in the bowl is correctly reconstructed to the water image. IDEAL, Iterative Decomposition with Echo Asymmetry and Least squares estimation; MRS, magnetic resonance spectroscopy.

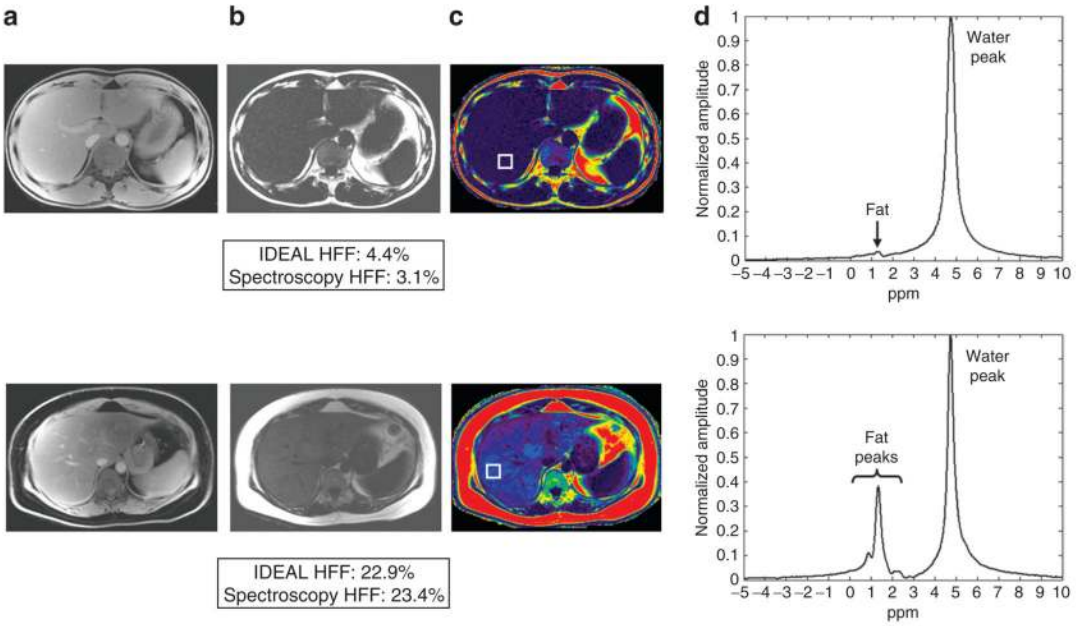

Figure 2.

Two examples of hepatic fat fraction (HFF) results from IDEAL and MRS. IDEAL-reconstructed (**a**) water, (**b**) fat, (**c**) fat fraction images are shown, along with (**d**) MRS plots. White boxes in (**c**) indicate location of the MRS voxel. IDEAL and MRS fat fractions agree closely in both subjects. Same color map is used from Figure 1. IDEAL, Iterative Decomposition with Echo Asymmetry and Least squares estimation; MRS, magnetic resonance spectroscopy.

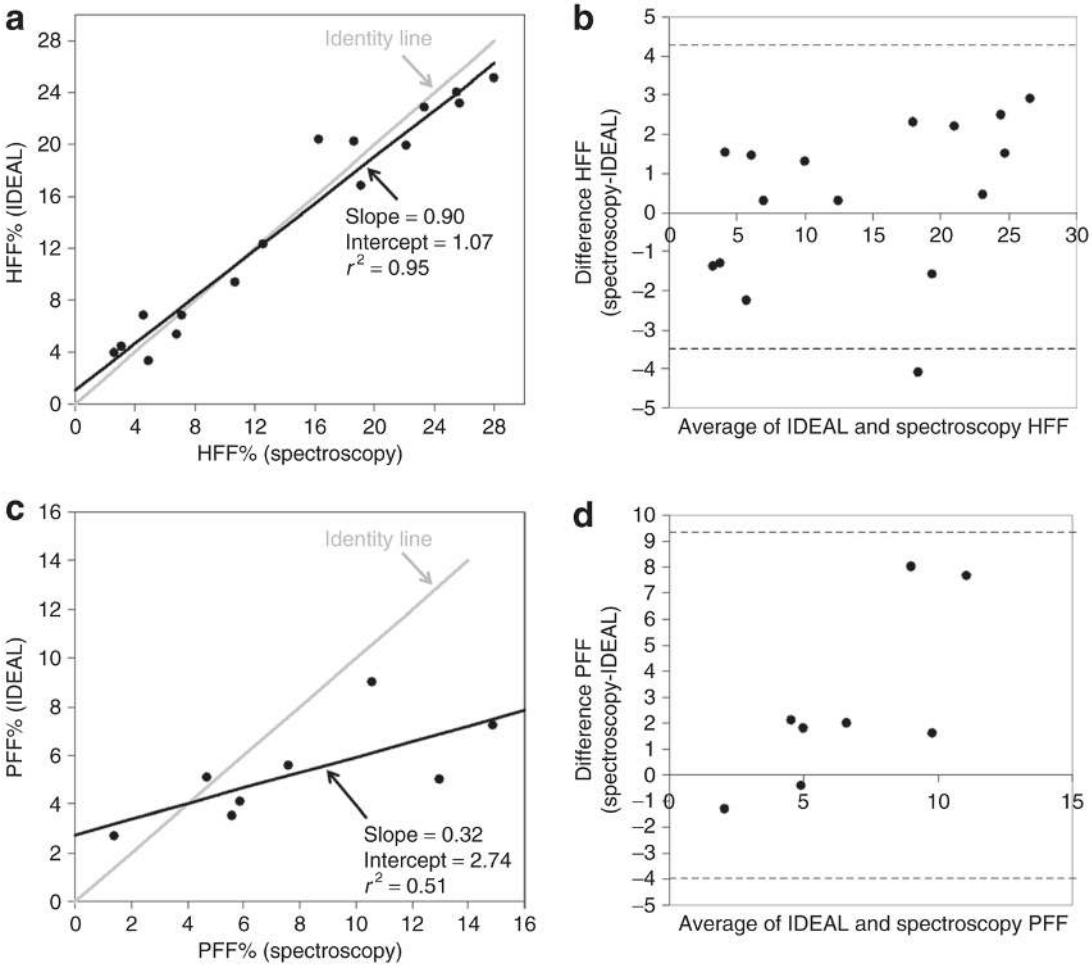

Figure 3.

(**a**) Correlation of hepatic fat fraction (HFF) between IDEAL and MRS in 16 studies. (**b**) Bland–Altman plot, with dashed lines representing the 95% confidence interval. (**c**) Correlation of pancreatic fat fraction (PFF) between IDEAL and MRS in 8 studies. (**d**) Corresponding Bland–Altman plot with dashed lines representing the 95% confidence interval. IDEAL, Iterative Decomposition with Echo Asymmetry and Least squares estimation; MRS, magnetic resonance spectroscopy.

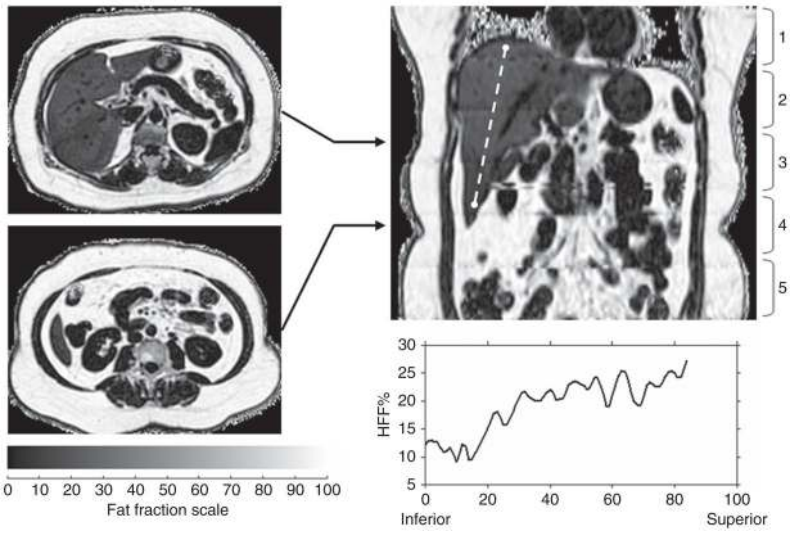

Figure 4.

Single reformatted coronal slice (fat fraction map) from five sets of axial acquisitions, showing contiguous coverage of the whole abdomen. Two source axial images are shown, one at the level of the liver and pancreas, and one at the level of the kidneys. Each axial acquisition was obtained in a 20-s breath-hold, acquiring a small slab as shown along the right. Profile along the dashed white line illustrates nonuniform fat fraction across the liver, highlighting the potential for IDEAL to detect heterogeneous organ fat infiltrations. The profile does not cross any hepatic vascular structures. Note the clear delineation of subcutaneous and visceral adipose tissue depots, along with fat fraction representation of major abdominal organs. HFF, hepatic fat fraction; IDEAL, Iterative Decomposition with Echo Asymmetry and Least squares estimation.